The North American Monsoon in the AR4 20C3M Simulations

Kenneth E. Kunkel, Xin-Zhong Liang, and Jinhong Zhu
Illinois State Water Survey • Champaign, IL

Introduction

The North American Monsoon (NAM) is of singular importance for water supplies in many parts of Mexico, particularly the northwest, and is a notable feature of the climate of the Southwest U.S. (Douglas et al., 1993; Higgins et al. 1999, Cavazos et al. 2002). In the core monsoon region of northwest Mexico, it typically arrives in June and retreats in September and accounts for a large fraction of annual precipitation.

We conducted a diagnostic analysis of model simulations regarding their ability to reproduce the surface climatic and tropospheric circulation features of the NAM. We identified key circulation features correlated with the interannual variability of June-September precipitation in the core NAM area of Mexico. We analyzed 55 20C3M simulations produced for the IPCC Fourth Assessment Report, comparing observed correlation patterns with those produced by the models.

North American Monsoon climatology

A region centered on northwest Mexico was defined as the core monsoon region (Fig. 1). The seasonal cycle of average (1961-1990) precipitation (Fig. 2) indicates a pronounced summer peak. The monsoon begins in late June (Englehart and Douglas 2006) and continues into early September.

There is a pronounced temporal correlation of inter-seasonal precipitation fluctuations and upper tropospheric flow patterns. Figure 3 shows the spatial pattern of the correlation between the time series of monthly precipitation in the core monsoon region (Fig. 1) and the time series of the monthly mean v component of wind at the 200 hPa pressure level. In June and September, there are strong positive correlations over extreme northwest Mexico/ southwest U.S., indicating that wet months are associated with anomalous southerly flow over this region. In July and August, there are negative correlations over eastern Mexico extending into the southwest U.S.

Correlations of the monthly precipitation time series with surface temperature (Fig. 4) indicate that wet (dry) months are associated with positive (negative) SST anomalies in the eastern Pacific off the west coast of Mexico in all monsoon months, although the location of maximum correlations shifts.

Performance of AR4 models

The diurnal cycle in the AR4 models is highly variable (Fig. 5). In many models, there is too much precipitation and the warm season begins earlier and/or extends later than observed, that is, the seasonal peak is longer than observed.

An examination of individual models illustrates the wide variations. The diurnal cycle is best represented in the ensemble members of the MRI model (Fig. 6). The NCAR PCM and CCSM exhibit positive biases and earlier onsets compared to observations (Fig. 7). The GFDL models exhibit a later retreat (Fig. 8) while one GISS model has no monsoon feature and another GISS model exhibits an earlier onset (Fig. 9).

Monthly time series of precipitation averaged over the core monsoon region were correlated with time series of the monthly v component at 200 hPa averaged over the regions in Fig. 3 with high correlations (extreme northwest Mexico/southwest U.S. in June and September and eastern Mexico in July and August). Figure 10 shows these correlation coefficients for each model simulation for the months of June, July, August, and September. For June, the observed correlation coefficient is +0.44. More than half of the simulations have coefficients of +0.3 or higher. For July, only nine simulations have coefficients less than -0.4, compared to the observed value of -0.59. Four of these simulations are from the MRI model. For August, 14 simulations have coefficients less than -0.4, compared to the observed value of -0.60, including all 5 MRI simulations. For September, only nine simulations have coefficients as high as +0.50, compared to the observed value of +0.68.

Monthly time series of precipitation averaged over the core monsoon region were correlated with time series of the monthly SST anomalies averaged over the east Pacific regions in Fig. 4 with high correlations. Figure 11 shows these correlation coefficients for each model simulation for the months of June, July, August, and September. For June, the observed correlation coefficient is +0.39. Fifteen of the simulations have coefficients of +0.3 or higher. For July, only four simulations have coefficients of +0.3 or higher, compared to the observed value of +0.46. For August, 11 simulations have coefficients of +0.2 or higher, compared to the observed value of +0.24. For September, ten simulations have coefficients as high as +0.2, compared to the observed value of +0.25.

Conclusions

Many models have difficulty reproducing the principal climate features of the NAM. The MRI model performs best, producing a very good seasonal cycle and relatively good correlations with observed upper tropospheric flow features. A number of the models capture the positive correlation with SSTs in June, but correlations in other months are generally not very close to the observed values.

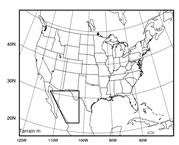

FIGURE 1
Box indicates the area identified in this study as the core monsoon region.

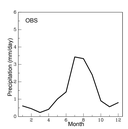

FIGURE 2
Observed mean monthly precipitation (mm/day) in the core monsoon region.

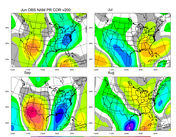

FIGURE 3
Correlation coefficient between the time series of monthly precipitation in the core monsoon region and the time series monthly average southerly wind component at 200 hPa. Time series cover the period 1961-1990.

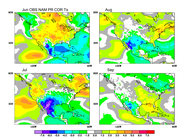

FIGURE 4
Correlation coefficient between the time series of monthly precipitation in the core monsoon region and the time series monthly of surface temperature. Time series cover the period 1961-1990.

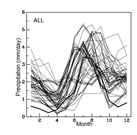

FIGURE 5
Annual cycle of monthly averaged (1961-1990) precipitation from observations (thick line) and the IPCC AR4 model 20C3M simulations.

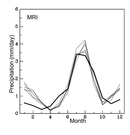

FIGURE 6
Annual cycle of monthly averaged (1961-1990) precipitation from observations (thick line) and the ensemble members of the MRI CGCM 2.3.2a model.

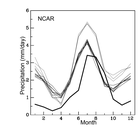

FIGURE 7
Annual cycle of monthly averaged (1961-1990) precipitation from observations (thick line) and the ensemble members of the NCAR PCM (dashed) and CCSM 3.0 (solid) models.

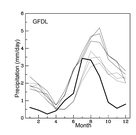

FIGURE 8
Annual cycle of monthly averaged (1961-1990) precipitation from observations (thick line) and the ensemble members of the GFDL CM2.0 (dashed) and CM2.1 (solid) models.

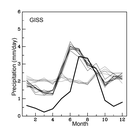

FIGURE 9
Annual cycle of monthly averaged (1961-1990) precipitation from observations (thick line) and the ensemble members of the GISS E-H (dashed) and E-R (solid) models.

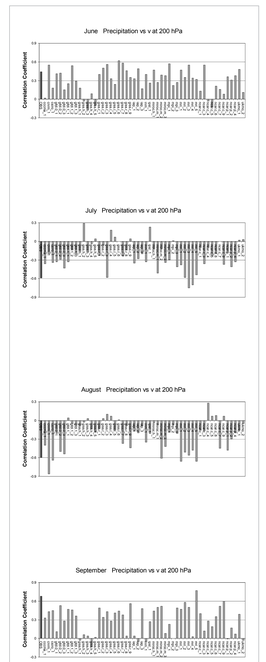

FIGURE 10
Correlation coefficient between the time series of monthly precipitation in the core monsoon region and the time series of the southerly wind component at 200 hPa for observations and for each model simulation for the months of June, July, August, and September.

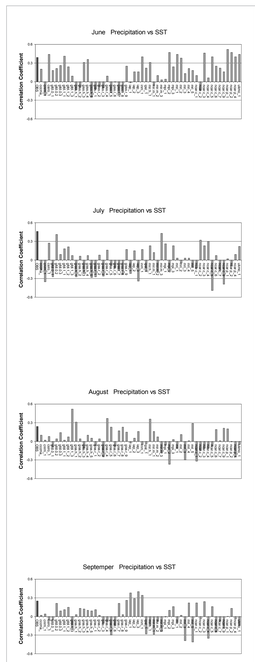

FIGURE 11
Correlation coefficient between the time series of monthly precipitation in the core monsoon region and the time series of monthly SST anomalies in the eastern Pacific for observations and for each model simulation for the months of June, July, August, and September.

REFERENCES
Cavazos, T., A. C. Comrie and D. M. Liverman, 2002: Intraseasonal variability associated with wet monsoons in southeast Arizona. *J. Climate*, **15**, 2477-2490.
Douglas, M.W., R.A. Maddox, K. Howard, and S. Reyes, 1993: The Mexican monsoon. *J. Climate*, **6**, 1665-1677.
Englehart, P.J. and A.V. Douglas, 2006: Defining intraseasonal variability within the North American monsoon. *J. Climate*, **19**, 4243-4253.
Higgins, R.W., Y. Chen and A.V. Douglas, 1999: Interannual Variability of the North American Warm Season Precipitation Regime. *J. Climate*, **12**, 653-680.

Illinois State WATER Survey (1895)
ILLINOIS DEPARTMENT OF NATURAL RESOURCES
1867